Simultaneous Improvement of Charge Generation and Extraction in Colloidal Quantum Dot Photovoltaics Through Optical Management

Havid Aqoma, Nilesh Barange, Ilhwan Ryu, Sanggyu Yim, Young Rag Do, Shinuk Cho, Doo-Hyun Ko, and Sung-Yeon Jang**

Inverted structure heterojunction colloidal quantum dot (CQD) photovoltaic devices with an improved performance are developed using single-step coated CQD active layers with a thickness of ≈60 nm. This improved performance is achieved by managing the device architecture to simultaneously enhance charge generation and extraction by raising optical absorption within the depletion region. The devices are composed of an ITO/PEDOT:PSS/PbS-CQD/ZnO/Al structure, in which the p–n heterojunction is placed at the rear (i.e., opposite to the side of illumination) of the devices (denoted as R-Cell). Sufficient optical generation is achieved at very low CQD layer thicknesses of 45–60 nm because of the constructive interference caused by the insertion of ZnO between the CQD and the Al electrode. The power conversion efficiency (PCE) of R-Cells containing a thin CQD layers (≈60 nm) is much higher (≈6%) than that of conventional devices containing CQD layers with a thickness of ≈300 nm (PCE ≈4.5%). This optical management strategy provides a general guide to obtain the optimal trade-off between generation and extraction in planar p–n junction solar cells. In terms of device engineering, all the layers in our R-Cells are fabricated using single coating, which can lead to compatibility with high-throughput processes.

1. Introduction

Colloidal quantum dots (CQDs) have emerged as one of the most promising photoactive materials for use in solar cell applications, since they are low-cost and solution processable. These materials also present unique advantages such as a band gap that is tunable using quantum size effects and multiple exciton generation.[1,2] Recent developments in understanding the chemistry of CQDs and device physics led to an increase in the power conversion efficiency (PCE) of CQD photovoltaic devices (CQDPVs) to approximately 9%.[3–5] An external quantum efficiency (EQE) of greater than 100% has also been demonstrated at particular wavelengths through multiple exciton generation.[6,7] Lead sulfide, PbS, is the most widely used material for high-performance CQDPVs, since its large Bohr radii (≈20 nm) can offer visible to near-infrared light absorption while assisting charge delocalization, which promotes mobility.[2,8,9] In addition, PbS CQDs can be easily synthesized to various sizes,[10] and are relatively robust during device fabrication under an air atmosphere. Solution-processed PbS-based CQDPVs were first demonstrated in 2005,[2] and have been widely investigated.[11]

Depleted p–n heterojunction devices employing n-type wide-band gap metal oxides (such as TiO_2 and ZnO) and p-type CQDs (such as PbS and PbSe) have been the most widely investigated, displaying state-of-the-art performances.[4,5,12] The depleted zone near a heterojunction provides efficient field-driven exciton (electron–hole pair) separation and electron extraction (**Figure 1**a,c). This zone also prevents the back-transfer of holes that could induce interfacial recombination due to the large discontinuity between the highest occupied molecular orbital (HOMO) of the CQDs and the valence band edge of n-type semiconductors.[13] In order to promote the efficient generation and extraction of electrons (the minority carriers), the heterojunction is normally located at the illuminating side (referred to as a front-side heterojunction cell, or F-Cell, in Figure 1a,b) because charge extraction in the quasi-neutral zone is much more inefficient

H. Aqoma, I. Ryu, Prof. S. Yim, Prof. Y. R. Do, Prof. S.-Y. Jang
Department of Chemistry
Kookmin University
77 Jeongneung-ro, Seongbuk-gu, Seoul 136-702, South Korea
E-mail: syjang@kookmin.ac.kr
N. Barange
Nano-Optical Property Laboratory and Department of Physics
Kyung Hee University
Seoul 130-701, South Korea
Prof. S. Cho
Department of Physics and EHSRC University of Ulsan
Ulsan 680-749, South Korea
Prof. D.-H. Ko
Department of Applied Chemistry
College of Applied Science
Kyung Hee University
1732 Deogyeong-dareo, Yongin-si, Gyeonggi-do 446-701, South Korea
E-mail: dhko@khu.ac.kr

DOI: 10.1002/adfm.201502664

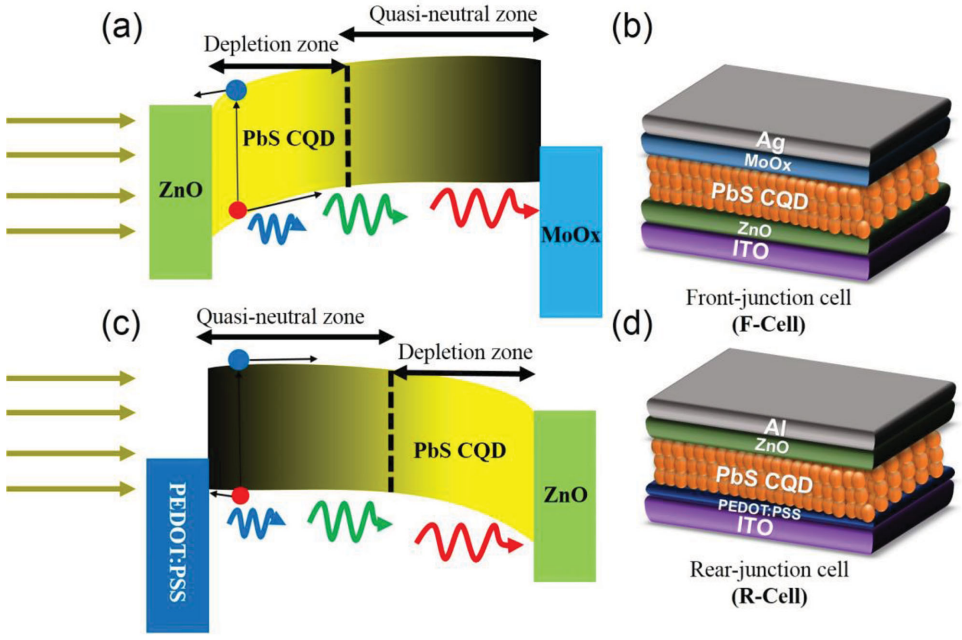

Figure 1. Schematic illustrations of the device operation mechanism and the device architectures of heterojunction colloidal quantum dot photovoltaic devices.

than that of the depletion zone. In this configuration, the PCE is generally optimized at a CQD layer thickness of a few hundred nanometers, as a result of the trade-off between exciton generation and charge extraction.[3,13–15] Improving the exciton generation within the region where charge extraction is efficient is a pertinent strategy in terms of addressing this trade-off and increasing the incident photon-to-current efficiency.

Enhancement of optical absorption within active layers of solar cells has been an effective strategy to improve device performance. The effects of optical enhancement using a spacing layer including thin ZnO layer have often been reported in the area of organic photovoltaic devices.[16–19] In CQDPVs, there has been recent efforts to enhance optical absorption within PbS CQD active layers either by forming microstructures,[5,20] or by developing novel CQDs with high absorption coefficients.[21] The judicious optical management within depletion zone of CQD layers will be a useful strategy to improve exciton generation in the devices.

In heterojunction CQDPVs, CQD active layers of the desired thicknesses are typically constructed using layer-by-layer (LBL) deposition methods.[22] In this case, a solution containing organic long-alkyl-chain (such as oleic acid, OA) capped CQDs[23] is used as a coating, followed by solid-state ligand-exchange using shorter bidentate molecules such as 3-mercapopropionic acid (MPA) or 1,2-ethanedithiol (EDT).[13,24] Conventional spin-coating or dip-coating methods may be used. After the ligand-exchange, CQD particles are cross-linked in order to yield insoluble continuous layers, enabling multiple LBL coating. The LBL method has become an essential technique in high-performance CQDPV fabrication, since it allows precise control of the active layer thickness.[3,6,11] Despite the fact that the LBL method offers an effective route for precise thickness manipulation, it relies on a tedious multiple-step process, typically involving 10–20 repeated rounds of coating and washing, which often hampers its application to high-throughput processes. Thus, the development of high-performance single-step fabricated CQD active layers will be very important in terms of device processing.

In this work, we fabricated heterojunction CQDPVs containing unusually thin CQD active layers (with a thickness of 45–60 nm), which were fabricated using a single-step deposition process. Improved exciton generation and charge extraction were simultaneously achieved in the thin PbS layers by placing a CQD/ZnO heterojunction at the opposite side of the device to illumination (referred to as the rear-side heterojunction cell, R-Cell, in Figure 1c,d). By inserting ZnO layers between the PbS CQD layer and an Al cathode to act as an optical spacer, optical absorption enhancement was realized. The optical properties of CQD layers were initially designed using finite-difference time-domain (FDTD) simulation, and then confirmed using experiment. The relationship between exciton generation and charge extraction in the R-Cells was investigated. In this configuration, the optimum trade-off between exciton generation and charge extraction occurred in very thin CQD layers (with a thickness between 45 and 60 nm). With the help of the high optical enhancement of the thin CQD layers, sufficient exciton generation was enabled within the thin layers. Furthermore, efficient charge extraction was simultaneously achieved due to the shorter distance for the charge to traverse, which may have been within the depletion zone. The PCE of the R-Cells containing CQD layers with a thickness of 60 nm was approximately 6%, which is significantly higher than that of optimized F-Cells containing CQD layers with a thickness of 300 nm (≈4.5%). It is of note that the high-performance thin CQD active layers in our R-Cells were fabricated using a simple single-step coating method, avoiding the LBL method.

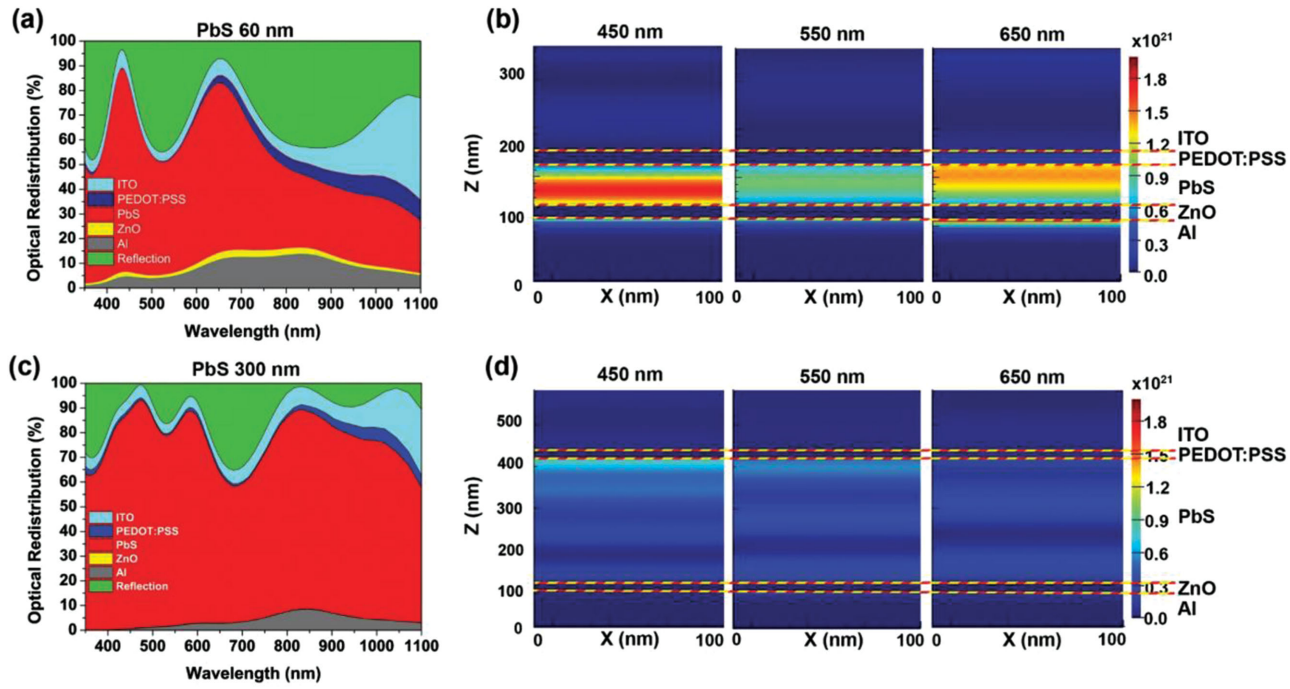

Figure 2. Optical simulation results obtained using finite-difference time-domain (FDTD). An R-Cell with PbS CQD active layers of a,b) 60 nm thickness and c,d) 300 nm thickness. The thickness of the ZnO, PEDOT:PSS, ITO, and Al layers were 20, 18, 150, and 100 nm, respectively. a,c) Optical redistribution and b,d) absorption per unit volume at particular wavelengths.

2. Results

2.1. Architecture and Fabrication of Rear-Side Heterojunction CQDPVs

The architecture of the R-Cells that were investigated in this study are shown in Figure 1d. For these R-Cells, a spin-coated PEDOT:PSS (≈18 nm thick) on an indium-doped tin oxide (ITO)/glass substrate was used as the hole-extraction layer. The PbS CQD and ZnO nanoparticles were successively spin-coated, followed by the deposition of a reflective Al cathode at reduced pressure, in order to produce devices containing an ITO/PEDOT:PSS/PbS CQD/ZnO/Al structure. The coating processes for the PbS/ZnO heterojunction were completed at low temperatures, under an ambient air atmosphere (at room temperature for the CQD layer, and at 75 °C for the ZnO layer). The cross-sectional scanning electron microscopy (SEM) image displayed in Figure S1a, Supporting Information, shows that each layer is evenly formed, with a clear distinction between layers. The PbS CQDs were synthesized using a conventional procedure detailed in the literature, with some modifications.[23] The band gap of the PbS CQDs used in the study was approximately 1.34 eV, as confirmed by the first excitonic peak in the solution UV–vis spectrum (Figure S1b, Supporting Information). The aqueous dispersible ZnO nanoparticles were synthesized via a solution-precipitation method reported previously.[25,26] In order to ensure a systematic study, we also fabricated conventional F-Cells to be used as control devices, using similar components (ITO/ZnO/PbS/MoOx/Ag, Figure 1b).[14,27–30]

2.2. Optical Simulation Studies in R-Cells

In order to understand the exciton generation profiles (i.e., the optical absorption) of CQD active layers in R-Cells upon illumination, the distribution of the optical fields was first simulated using commercially available FDTD software (Lumerical FDTD package). The optical constants of PbS, PEDOT:PSS, and ZnO were measured using variable-angle spectroscopy ellipsometry. The optical constants for PbS (refractive index, n, and extinction coefficient, k) are shown in Figure S2, Supporting Information. The optical constants for ITO and Al were obtained from the literature.[31,32] The thickness of each layer was taken from the cross-sectional SEM images of the devices (Figure S1a, Supporting Information), and these values were further confirmed by measuring layers coated individually under identical conditions (Figure S11, Supporting Information). The detailed calculation is shown in the Supporting Information.

As shown in **Figure 2**a,b and Figure S3, Supporting Information, the maximum generation rate within CQD active layers was enhanced by the inclusion of a ZnO layer of 20 nm thickness, indicating that the ZnO layer acted as an optical spacer. The calculated maximum J_{SC} values for R-Cells containing 60 nm thick CQD layers, using the simulated optical redistribution and exciton generation rate profiles, were enhanced by approximately 27% with the insertion of a 20 nm thick ZnO layer between the CQD and Al electrode (Table S1, Supporting Information). The calculated J_{SC} values of the R-Cells were higher when the ZnO thickness was 20–60 nm. Considering the electrical issues that may be in real devices, we chose

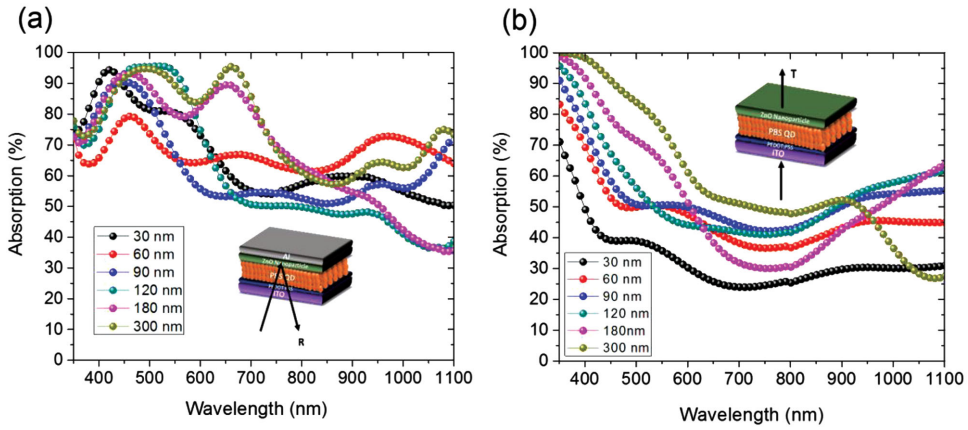

Figure 3. UV–vis spectra of R-Cells a) in reflectance mode and b) in transmittance mode.

20 nm thick ZnO spacer to simulate the exciton generation profiles at various CQD thicknesses. The results are shown in Figure 2 and Figure S4, Supporting Information. The calculated maximum J_{SC} values showed a continuous increase with increasing CQD layer thickness, as shown in Figure S5, Supporting Information.

2.3. Experimental Study of the Optical Properties of R-Cells

The absorption properties of CQD layers in R-Cells were investigated using UV–vis spectroscopy in order to confirm the validity of the simulated results. **Figure 3** displays the absorption spectra of R-Cells using two different measurement modes (reflectance mode and transmission mode). The scheme for each measurement are also depicted in the insets of Figure 3. The absorption spectra in transmission mode showed a near proportional increase in intensity as the CQD thickness increased at broad wavelengths (Figure 3b). However, the absorption spectra of the R-Cells in reflectance mode (Figure 3a) showed no particular dependency on thickness, and absorption was higher than in transmission mode. It is of note that relatively thin layers (30–60 nm) also showed sufficient absorption at broad wavelengths. This result is attributed to the fact that absorption in transmission mode (Figure 3b) results from single-path absorption, whereas in reflection mode (Figure 3a) it results from double-path absorption. The different absorption trends with respect to CQD thickness shown in Figure 3 are attributed to interference between the incident-path light and reflected-path light. The absorption profiles of R-Cells were enhanced across the whole wavelength range with the presence of a 20 nm thick ZnO optical spacer layer, confirming that there is indeed constructive interference (Figure S6, Supporting Information). This optical enhancement obtained through the insertion of the ZnO layer showed a good agreement with simulated results (Table S1, Supporting Information) and earlier studies, which reported on the active layers of organic photovoltaics.[16–19] The simulation and experimental studies were in good agreement, indicating that absorption of thin CQD layers can be enhanced by inserting a ZnO spacer between the CQD layer and the Al electrode, and that double-path absorption in thin CQD layers is sufficiently high.

2.4. Performance of CQDPVs

Figure 4 shows the photovoltaic performances of R-Cells with various CQD layer thicknesses and with 20 nm thick ZnO layers, and the resulting cell parameters are summarized in **Table 1**. The PCE and J_{SC} values reach their optimum at a CQD layer thickness of 45–60 nm, and exhibited a continuous decrease with increasing CQD thickness (Table 1 and Figure S7, Supporting Information). The J_{SC} values of R-Cells containing 300 nm thick CQD layers were ≈14% less than those of cells containing thin CQD layers. This optimized device performance with these thin CQD layers (45–60 nm) has never been presented in reported studies on CQDPVs, and differs from the trend of calculated maximum J_{SC} values of R-Cells (Figure S5, Supporting Information). Generally, J_{SC} values increase with increasing CQD layer thickness and reach an optimum value at >300 nm.[4,13,15,22] Despite the results of previous studies, our R-Cells achieved a sufficient photocurrent with CQD layer thicknesses of 45–60 nm.

Since identical symmetry-breaking interfacial layers (PEDOT:PSS and ZnO) were used for all our R-Cells, the photocurrent should be governed by exciton generation and charge extraction within the CQD active layers. The results of device analysis indicate that J_{SC} was optimized in relatively thin CQD layers, although the simulated J_{SC} profiles were continuously increasing with increasing CQD layer thickness (Figure S5, Supporting Information). This mismatch is due to the fact that in simulation, the maximum J_{SC} values were obtained using the exciton generation rate (Equation (3) in the Supporting Information), assuming a 100% charge collection efficiency. However, the measured J_{SC} values for the devices were determined using the product of the exciton generation rate and the charge collection efficiency. The charges from optically generated excitons should diffuse through the CQD layers to the corresponding electrodes, while also encountering electron–hole recombinations. The charges therefore have a restricted diffusion length within CQD layers.[3] The discrepancy between the simulated and measured current densities must stem from the disparity between the charge extraction efficiency in the R-Cells and ideal efficiency.

In order to further elucidate the charge collection efficiency of the R-Cells, the incident photon-to-current efficiency (IPCE)

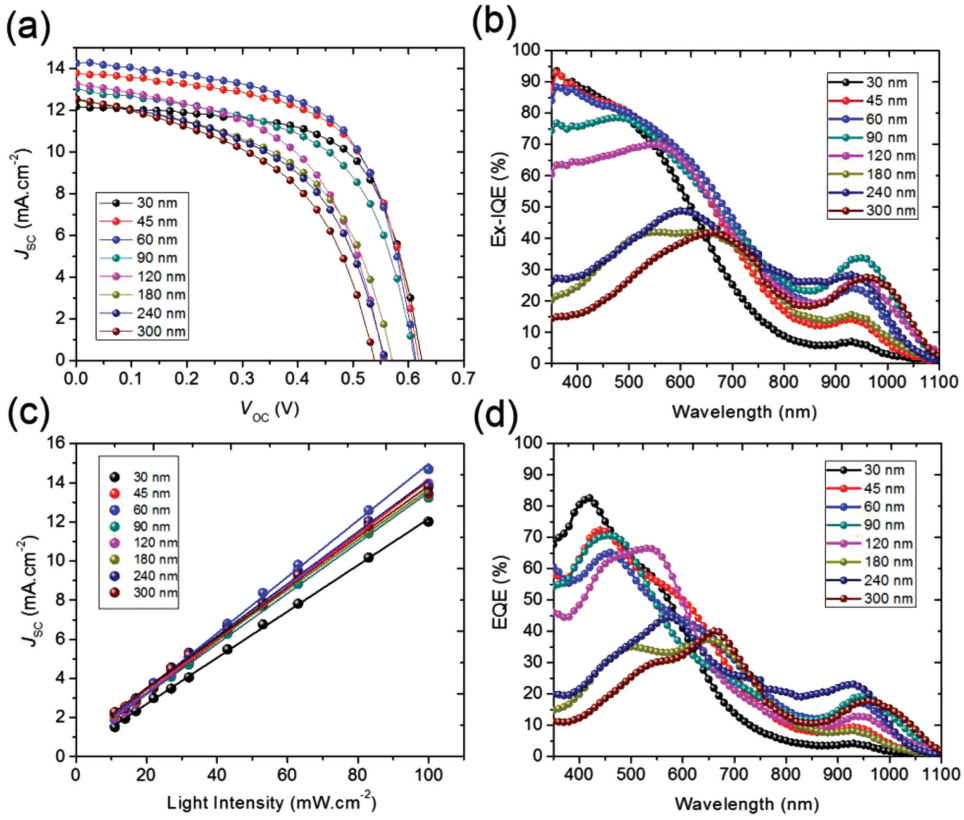

Figure 4. Performance of R-Cells with various PbS CQD active layer thicknesses. a) *J–V* characteristics, b) expanded internal quantum efficiency (Ex-IQE), c) short-circuit current density at various light intensities, and d) external quantum efficiency (EQE).

was investigated. The expended internal quantum efficiency (Ex-IQE) spectra (Figure 4b) clearly displayed significant changes in the IQE values with CQD thickness in the visible wavelength range. The Ex-IQE spectra were determined using the external quantum efficiency (EQE, Figure 4b) divided by [1-$R(h\nu)$], where $R(h\nu)$ is the reflectance at a photon energy of $h\nu$ (measured using an integrating sphere in order to include diffuse reflectance). This Ex-IQE usually represents the lower limit of the IQE, as it does not include a correction for light absorbed by other layers that do not contribute to the photocurrent.[33] The Ex-IQE value at visible wavelengths gradually reduced with increasing CQD thickness up to ≈120 nm, then was dramatically reduced for thicker layers (>120 nm). The Ex-IQE values for R-Cells at 400 nm containing 60, 120, 180, and 300 nm thick CQD layers were 86.6%, 64.4%, 24.5%, and 15.8%, respectively. This result indicated much higher charge extraction efficiency at thinner CQD layers. This result is in agreement with the continuous reduction in the FF values observed with increasing CQD layer thickness in R-Cells (Figure S7, Supporting Information).

Table 1. Summary of the performance parameters of R-Cells with various PbS CQD active layer thicknesses.

PbS thickness [nm]	PCE [%]	V_{OC} [V]	J_{SC} [mA cm^{-2}]	FF	R_{sh} [Ω]	R_s [Ω]	α
300	3.33	0.54	12.6	0.49	161	12.35	0.859
240	3.59	0.56	12.5	0.51	200	11.95	0.881
180	3.70	0.57	12.5	0.52	213	11.88	0.894
120	3.97	0.56	13.3	0.54	254	12.06	0.910
90	4.56	0.61	13.0	0.57	310	9.22	0.930
60	5.34	0.61	14.3	0.61	329	7.72	0.935
45	5.25	0.62	13.8	0.62	425	7.67	0.940
30	4.90	0.62	12.2	0.65	785	7.05	0.966

The charge extraction behaviors of R-Cells were further investigated using light intensity-dependent photovoltaic performance measurements (Figure 4c). A power law dependence of J_{SC} upon illumination intensity is generally observed in solar cells, and can be expressed as $J_{SC} \propto I^{\alpha}$, where I is the light intensity and α is the exponential factor.[34–36] The factor α approaches unity when bimolecular recombination is weakened during charge sweep-out. The fitted α values given in Figure 4c further deviated from unity for cells in which thicker CQD layers were used (Table 1). The α value for R-Cells with 60 nm thick CQD layers was 0.935, indicating that bimolecular recombination had little effect, although cells with approximately 120 and 300 nm thick CQD layers showed an increased bimolecular recombination, with α values of 0.910 and 0.859, respectively. This result indicated that bimolecular recombination within R-Cells in short-circuit conditions is enhanced as CQD thickness increases, which is responsible for reduced J_{SC}

and FF values. The reduction in the corresponding V_{OC} values further confirmed the presence of increased recombination, since identical active and charge collection layers (PbS CQDs, ZnO, and PEDOT:PSS) were used for all the R-Cells (Figure S7, Supporting Information). The evaluation and optimization of the FF, J_{SC}, and V_{OC} values of the R-Cells is further discussed in Section 3.

It is well known that the efficient charge extraction occurs within the CQDPV depletion zone, where the charges can be subject to carrier sweep-out with the help of the built-in potential.[13,37] The depth of the depletion zone can be measured using capacitance–voltage (C_p–V) characteristics. As shown in Figure S8 in the Supporting Information, the capacitance values at 0 V exhibited a continuous decrease for CQD thicknesses up to ≈120 nm, and maintained a constant level from ≈150 nm, which indicates the approximate depth of the depletion zone at a 0 bias (120–150 nm), under dark conditions.[38] We also calculated the depth of the R-Cell depletion zone. The calculated depth of the depletion zone was ≈110 nm, which shows reasonable agreement with experimental results obtained through C_p–V analysis. Details as to this calculation are given in the Supporting Information. The depletion zone depths for our R-Cells were similar to those reported by other groups, indicating that the PbS CQD and ZnO used in this study possess generally observed properties, and therefore that the observed optical enhancement will occur in most CQDPVs. Recently, there have been much efforts to improve optical properties in CQDPVs. The optical enhancement in the CQDPVs using microstructures have reported successfully improving device performance.[5,20] Separately, a chemical strategy to increase PbS quantum dot optical absorption coefficients was also suggested.[21]

Since the depth of the depletion zone shrinks upon the application of forward bias, the effective depth near the V_{OC} condition (or the maximum power point) would be reduced.[3] This result indicates that the origin of the drastic reduction of IQE and FF in R-Cells containing thick CQD layers may be attributed to the greatly enhanced recombination outside the depletion zone (i.e., in the quasi-neutral zone).[3]

2.5. Fabricating High-Performance CQDPVs Using a Single CQD Layer

Motivated by the superior exciton generation and charge extraction in a thin CQD layer, we attempted the fabrication of R-Cells using a single CQD layer. R-Cells containing CQD layers of approximately 60 nm thickness were prepared by both single-step and LBL coating methods, and their performances were compared. The J–V characteristics of these cells are shown in **Figure 5**a, and the resulting parameters are summarized in Table S3, Supporting Information. We successfully fabricated high-performance single-step coated CQD layers with the desired thickness (≈60 nm) by adjusting the coating conditions and the CQD solution concentrations. The performance of R-Cells that contained a single CQD layer was in fact superior

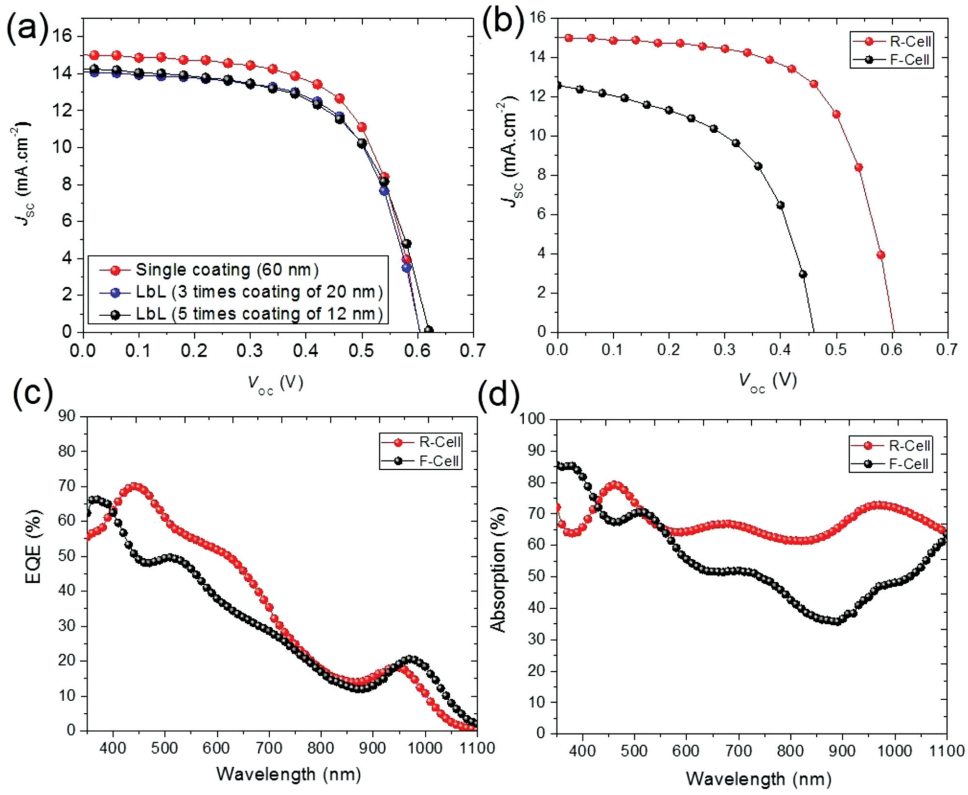

Figure 5. Performance of CQDPVs using a single-coated CQD active layer; a) J–V characteristics of R-Cells by various CQD layer preparation methods, b) J–V characteristics, c) EQE spectra, and d) UV–vis absorption spectra (transmission mode) of a R-Cell and a F-Cell using identical a single-coated CQD active layer. The thickness of PbS CQD layers was 60 nm. The J–V characteristics were measured under AM 1.5G 1 sun illumination (100 mW cm^{-2}).

to that of cells containing multiple CQD layers, deposited by LBL methods. Both the PCE and FF for R-Cells fabricated using the single-step coating method were higher (PCE: 5.82%. FF: 0.64) than those fabricated by LBL methods (PCE: 5.31%, FF: 0.60). We hypothesize that evasion of multiple ligand-exchange steps might reduce the density of surface-traps that may be generated by imperfect repassivation during exchange.[24] The maximum EQE was 70.1% at 440 nm. The PCE of single-coated R-Cells reached values of ≈6.3% (Figure S9, Supporting Information) in reduced light intensity conditions (20 mW cm^{-2}).

3. Discussion

Investigations into F-Cell architecture have dominated research into CQDPVs, due to advantages in terms of optical absorption near the p–n junction. Thicker CQD layers were preferred, though restricted charge diffusion limited the optimum thickness to approximately 300 nm.[13,39–41] The main reason for a lack of investigation into R-Cell architectures has been the reduced optical absorption near the p–n junction, which is located at the opposite side of the cell to illumination.[14,40,42,43] This logic is valid only if exciton generation relies mainly on the first-path light. However, in reality, absorption in these devices occurs through double-path absorption (through the first incident path and second reflected path), and therefore deliberate management in such a way that enables constructive interference can lead to dramatic improvements in total absorption. This fact enabled us to set the generation/extraction trade-off at a new optimization level as shown in Section 2. In order to further confirm the previous studies, we fabricated conventional F-Cells (control devices). The results were in accordance with previous literatures displaying the optimum PCE at a CQD thickness of ≈300 nm (4.54%, Figure S10, Supporting Information), which is much lower than that of R-Cells containing thinner (≈60 nm) CQD layers (5.82%). The detailed characterization results of the two types of devices containing identical single-step coated CQD layers (60 nm thick) are shown in Figure 5, and the resulting cell parameters are summarized in **Table 2**. The R-Cells displayed highly improved device performance, light absorption, and charge extraction compared to the F-Cells.

The tactical use of a dual-functioning ZnO layer between the PbS CQD layer and the Al cathode in this study offered both electronic and optical improvements to R-Cells by simultaneously enhancing charge generation and extraction. The optimized R-Cells showed far superior performances in terms of all their parameters compared to the optimized F-Cells (Table 1 and Table S4, Supporting Information), although R-Cells contained much thinner CQD layers (≈60 nm) than the F-Cells (≈300 nm). Once we compare these devices using 60 nm thick CQD layers, the PCE of the R-Cells (5.82%) was almost two times higher than that of the F-Cells (3.08%), indicating the importance of optical management in R-Cell architecture. The EQE spectra in Figure 4d further elucidate the uniqueness of the R-Cells. The peak in the EQE spectrum corresponding to 60 nm thick CQD-based R-Cells occurs at ≈450 nm, while the peaks corresponding to 120, and 300 nm thick CQD-based R-Cells are located at ≈550 and ≈650 nm, respectively. This result is attributed to a significant drop in the IQE at shorter wavelengths as CQD thickness increased, as shown in Figure 4b. Since high-energy photons (shorter wavelengths) are less penetrative than lower-energy photons (longer wavelengths),[41,44,45] the extraction of charges at shorter wavelengths becomes less and less efficient as CQD layer thickness increases. The optical simulation results in Figure 2b,d show results corresponding to the EQE spectra. In the case of thin CQD layer-based R-Cells (Figure 2b), absorption was well distributed throughout the CQD layers, regardless of wavelength, whereas in thick CQD layer-based R-Cells (Figure 2d), absorption at shorter wavelengths (450 and 550 nm) was more apparent near PEDOT:PSS/PbS junctions (opposite to the PbS/ZnO heterojunction). Absorption at relatively long wavelengths (650 nm) was distributed throughout the CQD layers for all layer thicknesses. This trend was confirmed for all the investigated CQD layer thicknesses, as shown in Figure S4, Supporting Information. Since the EQE values were determined using the product of the generation rate and the IQE, the significant reduction in charge extraction efficiency at shorter wavelengths due to charge recombination is the origin of the low J_{SC}, FF, and V_{OC} in thicker CQD layers. This work provides a general indication that optical management can be an efficient strategy for optimizing the trade-off between charge generation and extraction in p–n junction solar cells.

In terms of cell engineering, optimized CQD active layers for R-Cells (5.82% at 1 sun illumination and 6.3% at 0.2 sun illumination) can be achieved using a single-step coating method. This result is significant for adapting high-throughput processes and reducing material consumption when these processes are commercialized. There have been recent efforts to avoid multilayer LBL deposition processes,[46,47] but these methods have afforded only limited cell performances (PCE of 2.1%–2.4%), since the chemical process used to prepare single CQD layers yielded a higher trap-density. On the other hand, we used conventional chemical process for the CQD single layer preparation, which maintained good charge transport properties within the CQD layers. Our R-Cells are therefore by far the best performing CQDPVs fabricated using single-step coated CQD active layers.[46]

Table 2. Summary of the performance parameters of R-Cells and F-Cells with a single-coated PbS CQD active layer. The thickness of CQD layers was 60 nm.

Device	PCE max/average [%]	V_{OC} [V]	J_{SC} [mA cm^{-2}]	FF
R-Cells	5.82/5.51	0.60	15.01	0.64
F-Cells	3.08/3.01	0.46	12.58	0.53

4. Conclusions

Charge generation and extraction in CQDPVs were simultaneously improved through optical management of thin CQD active layers. Optical absorption within CQD layers was considerably enhanced by managing the device architecture in which a ZnO spacer that was placed near the Al electrode. Optimum trade-off between exciton generation and charge extraction

is achieved with a unusually thin CQD layer (thicknesses of 45–60 nm) as a result of sufficient optical generation due to constructive interference and efficient charge extraction. The PCE of R-Cells with ≈60 nm thick CQD layers (≈6%) was far higher than that of F-Cells with ≈300 nm thick CQD layers (≈4.5%). This work provides a general guide for optimizing the trade-off between charge generation and extraction in p–n junction solar cells. In terms of device engineering, all the layers in our R-Cells are fabricated using single coating, which could lead to compatibility with high-throughput processes.

5. Experimental Section

PbS Colloidal Quantum Dot Synthesis: PbS CQD was synthesized by following a previous reported method, with some modifications.[4] In brief, lead oxide (0.94 g, PbO, 99.99%, Sigma-Aldrich) and oleic acid (4 mL, OA, technical grade 90%, Sigma-Aldrich) were dissolved in 1-octadecene (20 mL, ODE, technical grade 90%, Sigma-Aldrich) at 109 °C, under vacuum conditions in a three-necked flask, for 2 h. The sulfur precursor solution was prepared by mixing TMS_2-S (360 µL, synthetic grade, Sigma-Aldrich) with ODE (10 mL). The sulfur solution was quickly injected into the reaction flask at 120 °C, waited for 1–2 s and followed by the injection of toluene (20 mL) for thermal quenching, after which the flask was cooled in a water bath. The PbS CQD was purified by precipitation at least once in acetone, and two or three times in toluene/methanol, using a centrifuge. After drying the residual solvent, PbS CQD was dissolved in octane at various concentrations.

Device Fabrication: ITO/glass was cleaned with acetone and isopropanol in sonication for 15 min, and then dried at 120 °C in a vacuum oven over night. After UV cleaning of the ITO for 20 min, Clevios AI4083 PEDOT:PSS purchased from H. C. Starck was diluted in MeOH (1/1 v/v) and spin-coated on the ITO/glass at 4000 rpm for 35 s, and then baked at 120 °C for 15 min. The PbS CQD solution (≈70 mg mL^{-1} for single coated active layer) was then spin-coated on the PEDOT:PSS layer at 2000 rpm for 10 s, and then 1,2-ethanedithiol (EDT, GC, >98 %, Fluka) in acetonitrile (2×10^{-3} M) was spin-coated on the PbS CQD layer. Washing twice with acetonitrile solution and then spinning was required in order to clean the residual EDT ligand. For CQD layers by LBL method, the coating of PbS CQD solutions (15–50 mg mL^{-1}, 2000 rpm) followed by EDT treatment were repeated until the desired thickness of CQD layers were obtained. ZnO nanoparticles were synthesized using a previously reported method.[26] ZnO nanoparticles (22 mg mL^{-1}) were spin-coated at 4000 rpm for 15 s, and heated to 75 °C for 5 min. All processes were performed in an air atmosphere. Finally, the 100 nm thick Al electrode was thermally evaporated onto the ZnO layer through a shadow mask in a high vacuum (<10^{-6} Torr). The deposited Al electrode area defined the active area of the devices to be 7.1 mm^2.

Characterizations: The *J–V* characteristics were measured using a Keithley 2401 source unit. Measurement was performed after 20 min of light soaking, for optimum performance. A solar simulator with a 150 W Xenon lamp (Newport) served as the light source. In order to minimize spectral mismatch, the light intensity was adjusted using monosilicon detectors, calibrated by the National Renewable Energy Laboratory (NREL). The light intensity was set to AM 1.5G. EQE measurements were performed using a 400 W Xenon lamp light source through a monochromator. The EQE measurement was performed without light soaking. The monochromated light was periodically interrupted at a frequency of 15 Hz, and compared to a reference silicon photodiode. Cross-sectional SEM images were taken using field-emission scanning electron microscopy (FE-SEM, JEOL JSM-7610F). Capacitance–voltage (C_p–V) measurements were performed using an impedance analyzer (IVIUM Tech., IviumStat). C_p–V sweeps were between −1 and 0.6 V, under the C_p–R_p model. The AC signal was set to 50 mV for amplitude voltage and 100 Hz for frequency.

FDTD Simulation: Finite-Difference time-domain simulations were carried out using the Lumerical FDTD software, version 8.11. SEM images were used for the structural dimensions and layer thicknesses. The optical constants of each layer obtained by ellipsometry were fed into the simulator. The periodic boundary conditions in the *x*, *y*-directions and perfectly matched layer (PML) boundary conditions in the *z*-direction were used with a plane wave light source. Absorption in each layer was calculated using the net transfer method. Calculation of generation rate was performed using a generation rate monitor. The optical constants of the PEDOT:PSS and PbS CQD layers were measured using ellipsometric data for wavelengths from 370 to 1200 nm (Variable incidence angle system (VASE) J.A. Woollam Co. Inc.). The optical constants for Al, ZnO, and ITO were used from literature.[31,32]

Supporting Information

Supporting Information is available from the Wiley Online Library or from the author.

Acknowledgements

The authors gratefully acknowledge support from the Basic Science Research Program and the Pioneer Research Center Program through the National Research Foundation of Korea (NRF-2012045675, S.-Y.J. and NRF-2013M3C1A3065033, D.-H.K.), New & Renewable Energy Core Technology Program of the Korea Institute of Energy Technology Evaluation and Planning (KETEP) granted financial resource from the Ministry of Trade, Industry & Energy, Republic of Korea (No. 20133030000210, S.-Y.J. and No. 20143030011530, D.-H.K.), and Global Scholarship Program for Foreign Graduate Students at Kookmin University in Korea. The portion of this research conducted at the University of Ulsan was supported by the National Research Foundation of Korea (Grant No. NRF-2013R1A2A2A01067741, S.C.).

Received: June 30, 2015
Revised: August 24, 2015
Published online: September 15, 2015

[1] V. K. Prashant, *J. Phys. Chem. C* **2008**, *112*, 18737.
[2] S. A. McDonald, G. Konstantatos, S. Zhang, P. W. Cyr, E. J. Klem, L. Levina, E. H. Sargent, *Nat. Mater.* **2005**, *4*, 138.
[3] D. Zhitomirsky, O. Voznyy, L. Levina, S. Hoogland, K. W. Kemp, A. H. Ip, S. M. Thon, E. H. Sargent, *Nat. Commun.* **2014**, *5*, 3803.
[4] C. H. M. Chuang, P. R. Brown, V. Bulovic, M. G. Bawendi, *Nat. Mater.* **2014**, *13*, 796.
[5] A. J. Labelle, S. M. Thon, S. Masala, M. M. Adachi, H. P. Dong, M. Farahani, A. H. Ip, A. Fratalocchi, E. H. Sargent, *Nano Lett.* **2015**, *15*, 1101.
[6] P. Maraghechi, A. J. Labelle, A. R. Kirmani, X. Lan, M. M. Adachi, S. M. Thon, S. Hoogland, A. Lee, Z. Ning, A. Fischer, A. Amassian, E. H. Sargent, *ACS Nano* **2013**, *7*, 6111.
[7] O. E. Semonin, J. M. Luther, S. Choi, H. Y. Chen, J. Gao, A. J. Nozik, M. C. Beard, *Science* **2011**, *334*, 1530.
[8] I. J. Kramer, E. H. Sargent, *ACS Nano* **2011**, *5*, 8506.
[9] J. E. Murphy, M. C. Beard, A. G. Norman, S. P. Ahrenkiel, J. C. Johnson, P. R. Yu, O. I. Micic, R. J. Ellingson, A. J. Nozik, *J. Am. Chem. Soc.* **2006**, *128*, 3241.
[10] M. Iwan, L. Karel, S. Dries, M. David De, N. Tom, C. M. José, V. Frank, V. André, D. Christophe, A. Guy, H. Zeger, *ACS Nano* **2009**, *3*, 3023.

[11] I. J. Kramer, E. H. Sargent, *Chem. Rev.* **2014**, *114*, 863.
[12] K. W. Kemp, A. J. Labelle, S. M. Thon, A. H. Ip, I. J. Kramer, S. Hoogland, E. H. Sargent, *Adv. Energy Mater.* **2013**, *3*, 917.
[13] A. G. Pattantyus-Abraham, I. J. Kramer, A. R. Barkhouse, X. H. Wang, G. Konstantatos, R. Debnath, L. Levina, I. Raabe, M. K. Nazeeruddin, M. Grätzel, E. H. Sargent, *ACS Nano* **2010**, *4*, 3374.
[14] G. H. Kim, B. Walker, H. B. Kim, J. Y. Kim, E. H. Sargent, J. Park, J. Y. Kim, *Adv. Mater.* **2014**, *26*, 3321.
[15] Z. J. Ning, O. Voznyy, J. Pan, S. Hoogland, V. Adinolfi, J. X. Xu, M. Li, A. R. Kirmani, J. P. Sun, J. Minor, K. W. Kemp, H. P. Dong, L. Rollny, A. Labelle, G. Carey, B. Sutherland, I. G. Hill, A. Amassian, H. Liu, J. Tang, O. M. Bakr, E. H. Sargent, *Nat. Mater.* **2014**, *13*, 822.
[16] J. Gilot, I. Barbu, M. M. Wienk, R. A. J. Janssen, *Appl. Phys. Lett.* **2007**, *91*, 113520.
[17] J. Y. Kim, S. H. Kim, H. H. Lee, K. Lee, W. L. Ma, X. Gong, A. J. Heeger, *Adv. Mater.* **2006**, *18*, 572.
[18] A. K. Kyaw, D. H. Wang, D. Wynands, J. Zhang, T. Q. Nguyen, G. C. Bazan, A. J. Heeger, *Nano Lett.* **2013**, *13*, 3796.
[19] S. H. Park, A. Roy, S. Beaupre, S. Cho, N. Coates, J. S. Moon, D. Moses, M. Leclerc, K. Lee, A. J. Heeger, *Nat. Photonics* **2009**, *3*, 297.
[20] A. J. Labelle, S. M. Thon, J. Y. Kim, X. Lan, D. Zhitomirsky, K. W. Kemp, E. H. Sargent, *ACS Nano* **2015**, *9*, 5447.
[21] C. Giansante, I. Infante, E. Fabiano, R. Grisorio, G. P. Suranna, G. Gigli, *J. Am. Chem. Soc.* **2015**, *137*, 1875.
[22] J. A. Tang, E. H. Sargent, *Adv. Mater.* **2011**, *23*, 12.
[23] M. A. Hines, G. D. Scholes, *Adv. Mater.* **2003**, *15*, 1844.
[24] D. A. Barkhouse, A. G. Pattantyus-Abraham, L. Levina, E. H. Sargent, *ACS Nano* **2008**, *2*, 2356.
[25] L. Qian, Y. Zheng, K. R. Choudhury, D. Bera, F. So, J. Xue, P. H. Holloway, *Nano Today* **2010**, *5*, 384.
[26] L. Qian, Y. Zheng, J. G. Xue, P. H. Holloway, *Nat. Photonics* **2011**, *5*, 543.
[27] H. Y. Park, I. Ryu, J. Kim, S. Jeong, S. Yim, S. Y. Jang, *J. Phys. Chem. C* **2014**, *118*, 17374.
[28] J. Gao, C. L. Perkins, J. M. Luther, M. C. Hanna, H. Y. Chen, O. E. Semonin, A. J. Nozik, R. J. Ellingson, M. C. Beard, *Nano Lett.* **2011**, *11*, 3263.
[29] B. Ehrler, K. P. Musselman, M. L. Bohm, F. S. F. Morgenstern, Y. Vaynzof, B. J. Walker, J. L. MacManus-Driscoll, N. C. Greenham, *ACS Nano* **2013**, *7*, 4210.
[30] J. M. Luther, J. B. Gao, M. T. Lloyd, O. E. Semonin, M. C. Beard, A. J. Nozik, *Adv. Mater.* **2010**, *22*, 3704.
[31] G. F. Burkhard, E. T. Hoke, M. D. McGehee, *Adv. Mater.* **2010**, *22*, 3293.
[32] E. D. Palik, *Handbook of optical constants of solids*, Vol. 3, Academic Press, MA, USA **1998**.
[33] O. E. Semonin, J. M. Luther, S. Choi, H. Y. Chen, J. Gao, A. J. Nozik, M. C. Beard, *Science* **2011**, *334*, 1530.
[34] S. R. Cowan, A. Roy, A. J. Heeger, *Phys. Rev. B* **2010**, *82*, 245207.
[35] V. D. Mihailetchi, H. X. Xie, B. de Boer, L. J. A. Koster, P. W. M. Blom, *Adv. Funct. Mater.* **2006**, *16*, 699.
[36] I. Riedel, J. Parisi, V. Dyakonov, L. Lutsen, D. Vanderzande, J. C. Hummelen, *Adv. Funct. Mater.* **2004**, *14*, 38.
[37] L. Xinzheng, M. Silvia, H. S. Edward, *Nat. Mater.* **2014**, *13*, 233.
[38] J. Tang, L. Brzozowski, D. A. R. Barkhouse, X. H. Wang, R. Debnath, R. Wolowiec, E. Palmiano, L. Levina, A. G. Pattantyus-Abraham, D. Jamakosmanovic, E. H. Sargent, *ACS Nano* **2010**, *4*, 869.
[39] D. A. R. Barkhouse, I. J. Kramer, X. H. Wang, E. H. Sargent, *Opt. Express* **2010**, *18*, A451.
[40] S. M. Willis, C. Cheng, H. E. Assender, A. A. R. Watt, *Nano Lett.* **2012**, *12*, 1522.
[41] J. Gao, J. M. Luther, O. E. Semonin, R. J. Ellingson, A. J. Nozik, M. C. Beard, *Nano Lett.* **2011**, *11*, 1002.
[42] W. L. Ma, S. L. Swisher, T. Ewers, J. Engel, V. E. Ferry, H. A. Atwater, A. P. Alivisatos, *ACS Nano* **2011**, *5*, 8140.
[43] J. M. Luther, M. Law, M. C. Beard, Q. Song, M. O. Reese, R. J. Ellingson, A. J. Nozik, *Nano Lett.* **2008**, *8*, 3488.
[44] M. Law, M. C. Beard, S. Choi, J. M. Luther, M. C. Hanna, A. J. Nozik, *Nano Lett.* **2008**, *8*, 3904.
[45] J. Nelson, *The Physics of Solar Cells*, Vol. 57, World Scientific, London, UK **2003**.
[46] A. Fischer, L. Rollny, J. Pan, G. H. Carey, S. M. Thon, S. Hoogland, O. Voznyy, D. Zhitomirsky, J. Y. Kim, O. M. Bakr, E. H. Sargent, *Adv. Mater.* **2013**, *25*, 5742.
[47] C. Giansante, L. Carbone, C. Giannini, D. Altamura, Z. Ameer, G. Maruccio, A. Loiudice, M. R. Belviso, P. D. Cozzoli, A. Rizzo, G. Gigli, *J. Phys. Chem. C* **2013**, *117*, 13305.